

# Feedbacks Between Hydrological Heterogeneity and Bioremediation Induced Biogeochemical Transformations

A. ENGLERT,<sup>\*†</sup> S. S. HUBBARD,  
K. H. WILLIAMS, L. LI, AND  
C. I. STEEFEL

Earth Sciences Division, Lawrence Berkeley National  
Laboratory

Received November 26, 2008. Revised manuscript received  
May 22, 2009. Accepted June 2, 2009.

For guiding optimal design and interpretation of in situ treatments that strongly perturb subsurface systems, knowledge about the spatial and temporal patterns of mass transport and reaction intensities are important. Here, a procedure was developed and applied to time-lapse concentrations of a conservative tracer (bromide), an injected amendment (acetate) and reactive species (iron(II), uranium(VI) and sulfate) associated with two field scale biostimulation experiments, which were conducted successively at the same field location over two years. The procedure is based on a temporal moment analysis approach that relies on a streamtube approximation. The study shows that biostimulated reactions can be considerably influenced by subsurface hydrological and geochemical heterogeneities: the delivery of bromide and acetate and the intensity of the sulfate reduction is interpreted to be predominantly driven by the hydrological heterogeneity, while the intensity of the iron reduction is interpreted to be primarily controlled by the geochemical heterogeneity. The intensity of the uranium(VI) reduction appears to be impacted by both the hydrological and geochemical heterogeneity. Finally, the study documents the existence of feedbacks between hydrological heterogeneity and remediation-induced biogeochemical transformations at the field scale, particularly the development of precipitates that may cause clogging and flow rerouting.

## Introduction

Biostimulation involves the injection of amendments into the subsurface to encourage in situ bacteria to degrade or transform contaminants to a less harmful or less mobile state (1). Although conceptually simple, biostimulation efficacy can be influenced by the ability to distribute injected amendment through the contaminated region and to maintain favorable hydrobiogeochemical conditions. In practice, ensurance of these conditions can be challenging, since natural variations in subsurface hydrological and biogeochemical properties exist that influence the location and magnitude of the induced reactions (2, 3).

Bioclogging, intensively studied over the last 20 years (4), has potential to further impact bioremediation efforts. Examples of biostimulation induced end-products include precipitates, gases, or biomass. As these products accumulate,

the potential of clogging the pore space or throats arises. If significant enough, these physical changes in the subsurface system can alter flow and transport characteristics, which in turn have the potential to influence where subsequent injected amendment can be delivered and where biogeochemical transformations occur. Such changes in flow and transport characteristics due to the formation of reaction end products are well studied and documented for laboratory scale experiments (5, 6) and through synthetic experiments (7, 8), but are largely unstudied at the field scale (4). Only a few studies have been performed that have documented field scale transformations associated with biostimulation. For example in advance of and during a biostimulation experiment performed at a DOE uranium(VI)-contaminated aquifer in Oak Ridge, TN, a forced gradient tracer test was performed (9). Bromide breakthrough curves associated with these tests revealed different responses as a function of time. Similarly, bromide breakthrough data collected in association with a chromium(VI) biostimulation study at the DOE Hanford 100H site revealed different responses as a function of time (10). Although these studies suggest that the borehole or aquifer conditions were altered by the biostimulation treatments, the data sets were neither analyzed to assess the spatiotemporal changes in flowpaths or reaction product distributions nor used to assess field-scale feedbacks.

Here, we explore time-lapse solute concentrations of injected amendments, reactants and end-products associated with two field scale biostimulation experiments that were successively conducted in 2002 and 2003 within a single experimental setup at the Department of Energy (DOE) Integrated Field Research Challenge Site (IFRC) at Rifle, Colorado. The ongoing work within the DOE U(VI)-contaminated aquifer at the Rifle IFRC site focuses on investigating the efficacy of biostimulation for facilitating microbial reduction of U(VI) to U(IV) through injection of acetate as electron donor. Previous research demonstrated that in some monitoring wells, the decline of U(VI) concentrations to below MCL in as little as nine days (11, 12). Two dimensional reactive transport models, developed for the Rifle IFRC site (13), have been used to synthetically explore the effects of physical and chemical heterogeneities on the transformation of mineral phases and spatial patterns of biomass accumulation. Simulations from these models suggest that the volume of the evolved iron sulfides, calcite, and biomass can total up to 5.5% of the pore space (14).

The aim of the present study is to analyze the time-lapse solute concentrations, acquired during the 2002 and 2003 biostimulation experiments at the Rifle IFRC site, to characterize the spatial distributions of bromide, acetate amendment, and reaction products at the field scale. With this information, we explore the dependencies of reactive species on amendment delivery and their change over time. To meet this objective, we draw in principle on the temporal moment analysis of locally measured bromide breakthrough curves (15, 16) and previously developed streamtube approach for representing flow and transport through a transect perpendicular to the mean flow direction (17, 18). However, we extend these approaches to estimate the accumulated response of the complex subsurface as a function of the injection of amendments. We utilize the new approach to gain insights about the interactions between subsurface heterogeneity and nonreactive as well as reactive transport. This understanding is expected to be helpful for guiding the design of in situ subsurface manipulations, such as those used to remediate contaminants, enhance oil recovery, and sequester carbon dioxide.

<sup>\*</sup> Corresponding author e-mail: Andreas.Englert@rub.de.

<sup>†</sup> Now at Applied Geology Department, Bochum University.

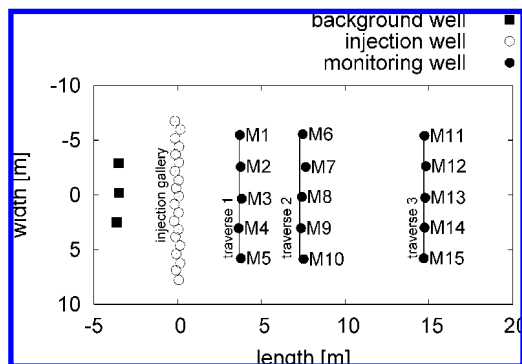


**FIGURE 1. Planview geometry of the 2002/2003 experiment at the Rifle IFRC site. Mean flow direction is roughly from left to right.**

In the following sections, we describe the procedure for the estimation of accumulated responses of conservative and reactive species as function of the injection and heterogeneity. We apply the procedure to bromide, acetate, iron, uranium, and sulfate measurements collected during the 2002 and 2003 biostimulation experiments at the Rifle IFRC site. We then compare the spatial patterns of accumulated responses and their changes over time. The present study is, to our knowledge, the first systematic analysis of time-lapse concentration data to assess field-scale feedbacks associated with a biostimulation field experiment.

## Materials and Methods

In the following section we first describe the general setup of the field biostimulation experiments and the biogeochemical reaction network. We present then a moment based approach to analyze the time-lapse concentrations of conservative and reactive species to estimate the spatial distribution of velocities and accumulated responses as function of the injection and the subsurface heterogeneity.

**Experimental Design.** Our study focuses on experiments collected within the 2002/2003 experiment (Figure 1) at the Rifle IFRC site. The subsurface hydrogeology germane to the biostimulation experiments at the Rifle IFRC site can be divided into three units. The deeper unit is an Eocene floodplain deposit called the Wasatch formation, which consists of silty shales of low permeability. At a depth of  $\sim 6.25$  m below ground surface, the Wasatch formation is overlain by a  $\sim 4.5$  m thick alluvial formation of Quaternary age that includes sandy gravely unconsolidated sediments with variable clay content. The shallowest unit is about  $\sim 1.75$  m thick and consists of a heterogeneous artificial fill of silty sandy sediments that includes a variable content of gravel and clay (11, 12). The water table (about 5 m below surface), located in the alluvial formation, represents the top of the shallow unconfined alluvial aquifer within which the biostimulation experiments were performed. The aquifers' average porosity was 0.27 (11). Annual changes in precipitation, snowfall, and snowmelt govern the recharge of the watershed. This results in annual groundwater level variations up to  $\sim 1.2$  m at the Rifle IFRC site. In the two experiments, the average hydraulic gradients were similar (2002: 0.0039 m/m, 2003: 0.0036 m/m) and roughly aligned with the long axis of the experiment (average deviation from long axis direction in 2002:  $15^\circ$ , 2003:  $13^\circ$ ). Results of detailed analysis of the gradients are provided in Supporting Information (SI) Figures SI-2–SI-4.

Utilized within the experiment were 3 upgradient wells, 20 injection wells, and 15 downgradient monitoring wells aligned over three rows (Figure 1). These wells (inner diameter 5.08 cm) were installed to a depth of 6.1 m and were screened along the entire saturated zone of interest from 1.5 to 6.1 m

(11, 12). At the injection wells, the coinjected bromide ( $\sim 84$  mol in 2002 and 2003) and acetate ( $\sim 881$  mol in 2002 and  $\sim 2822$  mol in 2003) was mixed with  $\sim 8500$  L of on site water from an upstream well in both experiments. During both experiments, this was accomplished by filling a stainless steel tank (2120 L) four times with the on-site water and adding each time  $\sim (1)/(4)$  of the total amount of bromide and acetate. From the tank, the bromide and acetate amended water was injected into the subsurface through the injection gallery. Here, each injection well was equipped with three injection ports, positioned at three different depth in the saturated zone. At each of the injection ports the prepared water was injected with an injection rate of  $\sim 1.2$  L/d over  $\sim 100$  days. Resulting bromide and acetate concentrations in the vicinity of the injection gallery was impacted by variations in the water level, the injection concentration, and the injection rate; field notes were used to estimate injection functions for the experiments (for details see SI Figure SI-5). Before, during, and after both experiments, the background and the monitoring wells were used to sample the groundwater over 260 days in 2002 and 220 days in 2003. Sampling of groundwater was performed in two steps. First, about 12 L groundwater were purged from the center of the water-column using a peristaltic pump until pH, dissolved oxygen, conductivity, and redox potential (all measured on surface with a multiprobe data sonde) stabilized. Second, the samples were collected with the same pumping equipment as during the purging procedure (11). Thereafter, groundwater samples were used to monitor solute concentrations of acetate, bromide, iron(II), uranium(VI), and sulfate (11, 12).

**Biogeochemical Reaction Network.** The experiments conducted in 2002 and 2003 both included a coinjection of acetate and bromide over a three-month period. The biogeochemical reaction network associated with these stimulations were developed using field and column data after (13, 14). Iron reduction is expected to occur first, reducing iron (hydro)oxide (represented by  $\text{FeOOH(s)}$  in SI Figure SI-6) to ferrous iron (Fe(II)) by iron reducing bacteria (*Geobacter* species, common in the Rifle subsurface). The iron reducer is expected to reduce aqueous U(VI) to immobile U(IV). After the depletion of "bioavailable" iron, sulfate is expected to be reduced by sulfate reducers (sulfate reducing proteobacteria), which should lead to the accumulation of aqueous S(-II) and eventually the formation of amorphous  $\text{FeS(am)}$  (11, 12). These biogeochemical reactions also produce bicarbonate, which can react with  $\text{Ca}^{2+}$  and  $\text{Fe}^{2+}$  species in the groundwater to produce precipitates, such as calcite ( $\text{CaCO}_3$ ) and siderite ( $\text{FeCO}_3$ ) (14). SI Figure SI-6 shows several major microbially mediated reactions and the associated mineral dissolution/precipitation reactions. A complete reaction network would also include surface complexation and aqueous speciation reactions.

**Analysis of Transport in a Bundle of Streamtubes.** In order to assess the spatiotemporal distributions of measured solutes in a naturally complex subsurface system, methods are needed to characterize multidimensional flow and transport in terms of meaningful parameters, often based on limited field observations. To meet this objective, we represent transport as a bundle of one-dimensional convective dispersive processes along an imaginary bundle of streamtubes (17–21). With this representation, flow and transport characteristics (for example, the pore velocity) are integrated over the distance between injection and observation well, rather than being a measure of a localized property. To distinguish the integrated transport characteristics from localized properties, we refer to the former as "apparent". As such, these apparent transport characteristics may change with distance from the injection, since the averaging volume of these apparent parameters changes with distance. As a consequence of the aquifer's heterogeneity, they may also

differ between different locations, even though the locations are equidistant from the injection. In this framework, a single bromide breakthrough curve represents the apparent result of a conservative transport process along a single streamtube. The spatial variability of the apparent transport characteristics can be assessed through analyzing several breakthrough curves from different observation wells along a traverse perpendicular to the mean flow direction. The temporal variability of apparent transport parameters can be assessed by analyzing consecutive experiments.

To estimate apparent parameters based on bromide breakthrough curves, we perform a temporal moment analysis (15). We expand the streamtube representation combined with temporal moment analysis in terms of an apparent accumulated mass, which is a flexible and quantitative estimate of the total amount of amendment delivered to a given monitoring location and the total amount of reactants and products, delivered after formation or consumption as result of biogeochemical reactions between injection and monitoring location. The apparent accumulated mass is based on the measure of the previously defined accumulated mass (16), but is modified here to allow for the quantitative characterization of conservative and reactive species in the framework of a streamtube approach. In the following, we first introduce the procedure to estimate temporal moments and the apparent velocity at a given location in the presence of a complex injection function. We subsequently describe the estimation of the apparent accumulated mass.

**Temporal Moment Analysis and Apparent Velocity Estimation.** To estimate the zeroth temporal moment ( $t_0$ ) (the area under a breakthrough curve) of bromide and acetate at each monitoring well we use a traditional approach:

$$t_0(x) = \int_0^{\infty} C(x, t) dt \quad (1)$$

where  $C$  is the solute concentration,  $x$  is the position in space, and  $t$  is the time. For example, the zeroth temporal moment of the bromide and acetate breakthrough curves at well M08 during the 2003 experiment are shown in pink in SI Figure SI-1c and d, respectively.

To estimate the zeroth temporal moment of iron(II), uranium(VI) and sulfate we used

$$t_0(x) = \int_0^{\infty} C(x, t) - C_b(x, t) dt \quad (2)$$

where  $C_b$  is the average background concentration, which was estimated based on the averaged measurements from the three upgradient background wells at each time step (Figure 1). The zeroth moments of iron(II), uranium(VI), and sulfate for the monitoring well M08 in the 2003 experiment are highlighted in pink in SI Figure SI-1e–g. The calculation of the zeroth moment based on eq 2 can either quantify reaction products with increased concentrations compared to a background concentration (as in the case of Fe(II) or reactants with decreased concentrations (as in the cases of U(VI) and sulfate). It is important to note that the estimate of  $t_0$  based on eq 2 is only valid if the injected water has a concentration similar to the background concentration  $C_b$ , as in the case of the Rifle experiments. Furthermore, the estimate of  $t_0$  based on eq 2 is only valid if the variation of the background concentration is small compared to the concentrations observed at a monitoring well and/or the duration of the experiment is long compared to the mean traveltime from the injection to the monitoring well.

To estimate the apparent velocity, we then calculated the first temporal moment ( $t_1$ ) of the bromide breakthrough curve, which is identical to the mean arrival time ( $\mu_t$ ) of bromide, following

$$t_1(x) = \mu_t(x) = \int_0^{\infty} t \frac{C(x, t)}{t_0} dt \quad (3)$$

For a Dirac pulse, the bromide travel time mean can be used to estimate  $v_a$  using a traditional approach ( $v_a = (d(x))/(\mu_t(x))$ ). However, in our case of a multistep pulse injection (e.g., SI Figures SI-1a,b and SI-5), it was necessary to take into account the first moment of the injection function in the estimation of  $v_a$ . To do this, we first estimated the first temporal moment of the injection function at the injection gallery ( $\mu_{t,INJ}$ ) and of the bromide breakthrough curves ( $\mu_{t,BTC}$ ) using eqs 1 and 3. We then calculated the difference between the mean of the injection time and the mean of the travel time,  $\mu_{t,step}$  for every bromide breakthrough data set:

$$\mu_{t,step}(x) = \mu_{t,BTC}(x) - \mu_{t,INJ} \quad (4)$$

We then calculated the apparent velocity over a distance,  $d$ , from the injection gallery to a given monitoring well by

$$v_a(x) = \frac{d(x)}{\mu_{t,step}(x)} \quad (5)$$

**Apparent Mass Estimation.** Previously published research (16) has described an accumulated mass ( $m_{(acc)}$ ) concept, which is an integrated measure of mass flux over time at a particular location. With this approach (16), the accumulated mass is calculated by taking the product of the zeroth temporal moment of a breakthrough curve and the local groundwater flux ( $Q$ ) at a position in space ( $m_{(acc)} = Q t_0$ ). This approach was previously applied to synthetic transport experiments (16), where the groundwater flux was known at every position in space. Although a valuable concept, this approach is difficult to apply to field data sets because the local groundwater flux is typically not known. However, if variations of the flow field in time are small during an experiment (as is the case at Rifle: SI Figures SI-2–SI-5), we can estimate a zeroth moment and apparent velocity at locations where a breakthrough curve of a conservative tracer is measured. Based on these estimates, we can derive an apparent accumulated mass ( $m_a$ ), or the accumulated mass per pore area integrated over a streamtube from the injection location to a given monitoring well. Synthetic studies of inert tracers have shown that the spatial velocity field is important for estimating the spatiotemporal distribution of solutes at cross sections perpendicular of the mean velocity (22, 23). These studies have also shown that the usage of the apparent velocity as a proxy for the local velocity can improve estimation of mass fluxes based on resident concentrations measured at monitoring wells during tracer experiments.

Here, we relate the groundwater flux,  $Q$  to the local pore velocity,  $v_p$ , by  $v_p = (Q)/(A\phi)$ , where  $A$  is the cross-sectional area and  $\phi$  is the porosity of the porous medium through which the groundwater travels. We can then calculate the accumulated mass (16) as  $m_{(acc)} = v_p A \phi t_0$ . Normalizing the accumulated mass by the porosity and the cross-sectional area, we define the accumulated mass per pore space ( $m_p$ ) as follows:

$$m_p(x) = \frac{m_{(acc)}(x)}{A(x)\phi(x)} \quad (6)$$

$$= v_p(x) t_0(x) \quad (7)$$

At an injection location, the accumulated mass per pore space can be estimated using eq 6, where the known total injected mass of a substance is  $m_{(acc)}$ , the area of injection is  $A(x)$  (in our case the length times the height of the injection gallery) and the porosity at the injection is  $\phi(x)$ . At monitoring wells, where  $m_{(acc)}$  is not known, one can instead utilize the apparent

velocity (using eqs 1, 3, 4, and 5) to estimate the apparent accumulated mass,  $m_a$  as

$$m_a(x) = v_a(x) t_0(x) \quad (8)$$

As with the apparent velocity, the apparent accumulated mass is also an integrated measure, since both the apparent velocity and the zeroth moment are a result of integrating processes along a streamtube from the injection to the point of monitoring. The apparent accumulated mass is an estimate of the total integrated mass passing an area  $A$  within a medium of porosity  $\phi$  during an experiment; its units are mass per area, and we refer to it in from here on as apparent mass ( $m_a[(\text{mol})/(\text{m}^2)]$ ).

To extend the concept of the apparent mass to reactive species, the approach must consider the nature of the species (i.e., conservative or not, injected or not, reactant or product). However, estimation of the apparent mass is straightforward (using eq 8) once the 0th temporal moment of the species and the collocated apparent velocity of the conservative tracer are calculated by eqs 1–5. For example, the apparent mass of bromide at a given location can be estimated by ( $m_a^{\text{bromide}}(x) = t_0^{\text{bromide}}(x) v_a^{\text{bromide}}(x)$ ) and the apparent mass of reduced sulfate can be estimated by ( $m_a^{\text{sulfate}}(x) = t_0^{\text{sulfate}}(x) v_a^{\text{bromide}}(x)$ ). The measure of the apparent mass of the coinjected species bromide and acetate also permits an estimate of the acetate's apparent consumption along a streamtube:

$$m_a^{\text{consumed acetate}}(x) = \frac{m_p^{\text{injecte acetate}}}{m_p^{\text{injecte bromide}}} \cdot m_a^{\text{bromide}}(x) - m_a^{\text{acetate}}(x) \quad (9)$$

where  $m_p$  for acetate and bromide can be estimated using eq 6 and  $m_a(x)$  can be estimated for acetate and bromide at monitoring wells using eq 8.

## Results

For both biostimulation experiments, the application of the temporal moment analysis (eqs 1, 3, and 4) to the time-lapse monitoring well bromide concentration data and to the estimated bromide injection function (at the injection gallery) permitted an estimate of the apparent velocity (eq 5) for all monitoring wells, except M10 and M15. The data from the two latter monitoring wells only allowed rough estimates, due to low/no bromide delivery at those locations. The zeroth temporal moments of the injected species (bromide and acetate, calculated using eq 1) and of other species (reduced uranium(VI), iron(II) and sulfate, calculated using eq 2) were used in eq 8 to estimate apparent masses ( $m_a$ ) for the same monitoring wells. Utilizing eq 6, we then estimated the accumulated mass of the acetate and bromide injection based on the known measures of the cross-sectional area of the injection gallery, the porosity of the aquifer and injected bromide and acetate masses during the two experiments. Based on acetate and bromide accumulated mass per pore space ( $m_p$ ) at the injection gallery together with  $m_a$  of acetate and bromide at monitoring wells, we estimated the  $m_a$  of consumed acetate using eq 9. As outlined in the prior sections,  $m_a$  can be a quantitative measure of both the accumulated appearance or disappearance of a substance. In the following,  $m_a$ , calculated based on aqueous concentration data, quantifies on the one hand the appearance of bromide, and reduced Fe(II), and on the other hand the accumulated disappearance of acetate through consumption and U(VI) and sulfate through reduction.

Both the mean of  $m_a$  ( $\mu(m_a)$ ) and the standard deviation of  $m_a$  ( $\sigma(m_a)$ ) within a control plane are shown in Figure 2 for the two experiments as a function of distance from the injection gallery. At the injection gallery (distance 0), we

utilized  $m_p$  as a proxy for  $m_a$  of the injected species, bromide and acetate. The  $m_a$  of the consumed acetate, and other reactive species (reduced Fe(II), U(VI), and sulfate) were assumed to be 0 at the injection gallery, since no biostimulation was performed upgradient the injection. At the downgradient traverses,  $\mu(m_a)$  and  $\sigma(m_a)$  are estimated by  $m_a$  values at M01–M05 (traverse 1), M06–M09 (traverse 2), and M11–M14 (traverse 3). Figure 2 is discussed in the following, while statistical analysis associated in the interpretation can be found in SI Tables SI-2 and SI-3.

Figure 2a shows the evolution of the  $\mu(m_a)$  of bromide as function of distance from the injection gallery. As bromide is inert, Figure 2a illustrates the overall conservative mass transport characteristics during the two biostimulation experiments. Variations in  $\mu(m_a)$  of bromide between traverses in both experiments indicate the hydrological heterogeneity of the subsurface, which is only roughly captured by five monitoring wells per traverse. For the bromide data, the ratio between  $\mu(m_a)$  at the injection gallery and  $\mu(m_a)$  at traverses expresses the estimated mass recovery during the experiments. Mass recovery (not shown) was ~60% at the first, ~100% at the second and ~75% at the third traverse. Figure 2a also shows that  $\sigma(m_a)$  is substantial in both experiments, especially along the second traverse. The values of  $\mu(m_a)$  and  $\sigma(m_a)$  of bromide were similar in the 2003 experiment compared to the 2002 experiment.

The  $\mu(m_a)$  of consumed acetate shows significantly higher values in the 2003 experiment compared to the 2002 experiment, which is a consequence of the (three times) higher acetate concentration used during the 2003 injection (Figure 2b). During both experiments,  $\mu(m_a)$  of consumed acetate increases with distance to the injection gallery until the second traverse. Further downgradient,  $\mu(m_a)$  of consumed acetate decreases slightly. The behavior of  $\mu(m_a)$  of consumed acetate is interpreted to be due to a combined effect of acetate consumption and the variability in the mass recovery. The rapid increase of  $\mu(m_a)$  of consumed acetate between the injection and the second traverse indicates that most acetate is consumed closer to the injection, which is consistent with reactive model simulations (14).

Figure 2c shows that the  $\mu(m_a)$  of reduced iron increases with distance to the injection in both experiments and that the variabilities of  $m_a$  of Fe(II) ( $\sigma(m_a)$ ) are high. The  $\mu(m_a)$  of Fe(II) is similar or slightly smaller in the 2003 experiment compared to the 2002 experiment. We interpret this result to be associated with the bioavailability of Fe(III), which limits iron reduction, although acetate delivery tripled. During both experiments, the  $\mu(m_a)$  of reduced sulfate increases between the injection and the first traverse (Figure 2e). The  $\mu(m_a)$  of reduced sulfate further increases significantly between the first and second traverse in 2003, before it decreases between the second and third traverse. In 2002, the  $\mu(m_a)$  of reduced sulfate reaches a plateau between the second and third traverse, before it decreases slightly toward the third traverse. The  $\mu(m_a)$  of reduced sulfate was distinctly higher in the 2003 experiment compared to the 2002 experiment, which we interpret to be due to the higher acetate delivery to the subsurface in 2003. In both experiments, we interpret the decrease of  $\mu(m_a)$  of reduced sulfate at further downgradient traverses to be a result of reduced mass recovery. The  $\mu(m_a)$  of reduced uranium increases with distance until the second traverse in both experiments (Figure 2d). Between the second and third traverse,  $\mu(m_a)$  of reduced uranium increased slightly in 2002, but decreased in 2003. We interpret the decrease in 2003 and the only slight increase in 2002 to be a result of reduced mass recovery. The  $\mu(m_a)$  of reduced uranium is higher in the 2003 experiment compared to the 2002 experiment at all traverses. Although we have not yet understood the biogeochemical mechanisms,

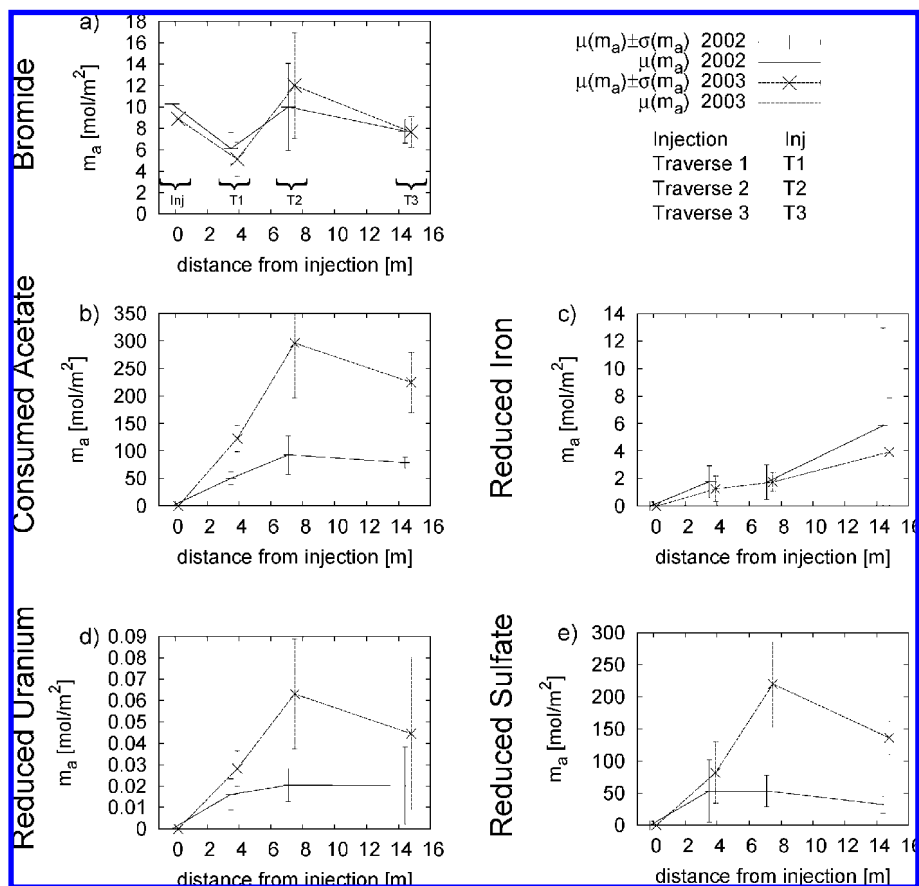


**FIGURE 2.** Statistics of the apparent accumulated mass (mean,  $\mu(m_a)$ , and standard deviation,  $\sigma(m_a)$ ) of several species as a function of distance from the injection gallery, as obtained from the two experiments at the Rifle IFRC 2002/2003 site: Figure a shows statistics of  $m_a$  as an estimate of the injected and delivered amount of bromide to a given gallery or traverse (T no.). Figure b shows the  $m_a$  statistics as an estimate of the amount of acetate consumed along the flowpaths to a given traverse. Panels c–e show statistics of  $m_a$  as an estimate of the amount of iron, uranium and sulfate reduced along the flowpaths to a given traverse. Traverses T1, T2, and T3 correspond to those indicated in Figure 1.

we speculate this to be a result of the higher acetate delivery in the 2003 experiment.

To explore the spatial patterns of mass transport and biogeochemical end-products, individual  $m_a$  values were normalized along traverses. We normalized  $m_a$  to extract the spatial behavior of  $m_a$  from the overall mass transport behavior (mass recovery) and to compare the spatial patterns of  $m_a$  associated with different species, whose  $m_a$  were of different orders of magnitude before the normalization procedure. For normalizing the individual  $m_a$  at monitoring locations along a given traverse we used  $m_a^{\text{norm}} = (m_a - \mu(m_a)) / (\sigma(m_a))$ . This procedure was carried out for each local  $m_a$  value using  $\mu(m_a)$  and  $\sigma(m_a)$  of the shared traverse. The  $m_a^{\text{norm}}$  were then linearly spatially interpolated to yield the images shown in Figure 3. In the following, we analyze and interpret the (dis)similarity in the patterns qualitatively using Figure 3 and quantitatively by using associated correlation coefficient ( $r$ ) (summary of the correlation coefficients given in SI Table SI-1).

Figure 3a and f show that significant differences ( $r = 0.23$ ) in the spatial patterns of the  $m_a^{\text{norm}}$  of bromide exist between the two experiments. Distributions of the  $m_a^{\text{norm}}$  of bromide generally coincide with the  $v_a$  distributions, whose values can vary by a factor two. Both the  $m_a^{\text{norm}}$  of bromide and the  $v_a$  show significant differences in their spatial patterns between the two experiments, indicating changes of the conservative transport behavior. Although different ( $r = 0.37$ ) between the two experiments, the spatial patterns of the  $m_a^{\text{norm}}$  of consumed acetate and the  $m_a^{\text{norm}}$  of bromide are similar ( $0.96 \leq r \leq 0.99$ ) in both experiments (Figure 3a, b,

f, and g). This was to be expected and shows that the consumption of acetate is strongly governed by conservative transport processes.

Figure 3c and h reveal that the patterns of the  $m_a^{\text{norm}}$  of reduced iron during the 2002 and 2003 experiment are similar ( $r = 0.80$ ). The dissimilarity ( $0.00 \leq r \leq 0.38$ ) between the patterns of the  $m_a^{\text{norm}}$  of consumed acetate and of the reduced iron in both experiments suggests the influence of the acetate delivery on the patterns of the iron reduction to be minor (Figure 3b, c, g, and h). This indicates that the intensity of the iron reduction is possibly governed by other factors, including geochemical heterogeneities (i.e., the distribution of “bioavailable” Fe(III) in the subsurface sediments). This observation is consistent with previous synthetic studies (2). Figure 3e and f reveal significant differences ( $r = 0.26$ ) in patterns of the  $m_a^{\text{norm}}$  of reduced sulfate between the 2002 and 2003 experiments, as was also observed for the  $m_a^{\text{norm}}$  of bromide and consumed acetate. However, the patterns of  $m_a^{\text{norm}}$  of reduced sulfate are similar ( $0.68 \leq r \leq 0.90$ ) to those of bromide and consumed acetate. These observations indicate that the intensity of the sulfate reduction is dominated by the delivery of acetate, which in turn is governed by conservative transport processes. Inspection of the patterns of the  $m_a^{\text{norm}}$  of reduced uranium indicates that the uranium reduction patterns were similar ( $r = 0.87$ ) for both experiments (Figure 3d and i). During the low acetate delivery in the 2002 experiment, the patterns of the  $m_a^{\text{norm}}$  of reduced uranium coincided ( $r = 0.73$ ) with those of the  $m_a^{\text{norm}}$  of reduced iron (Figure 3c and d). During high acetate delivery

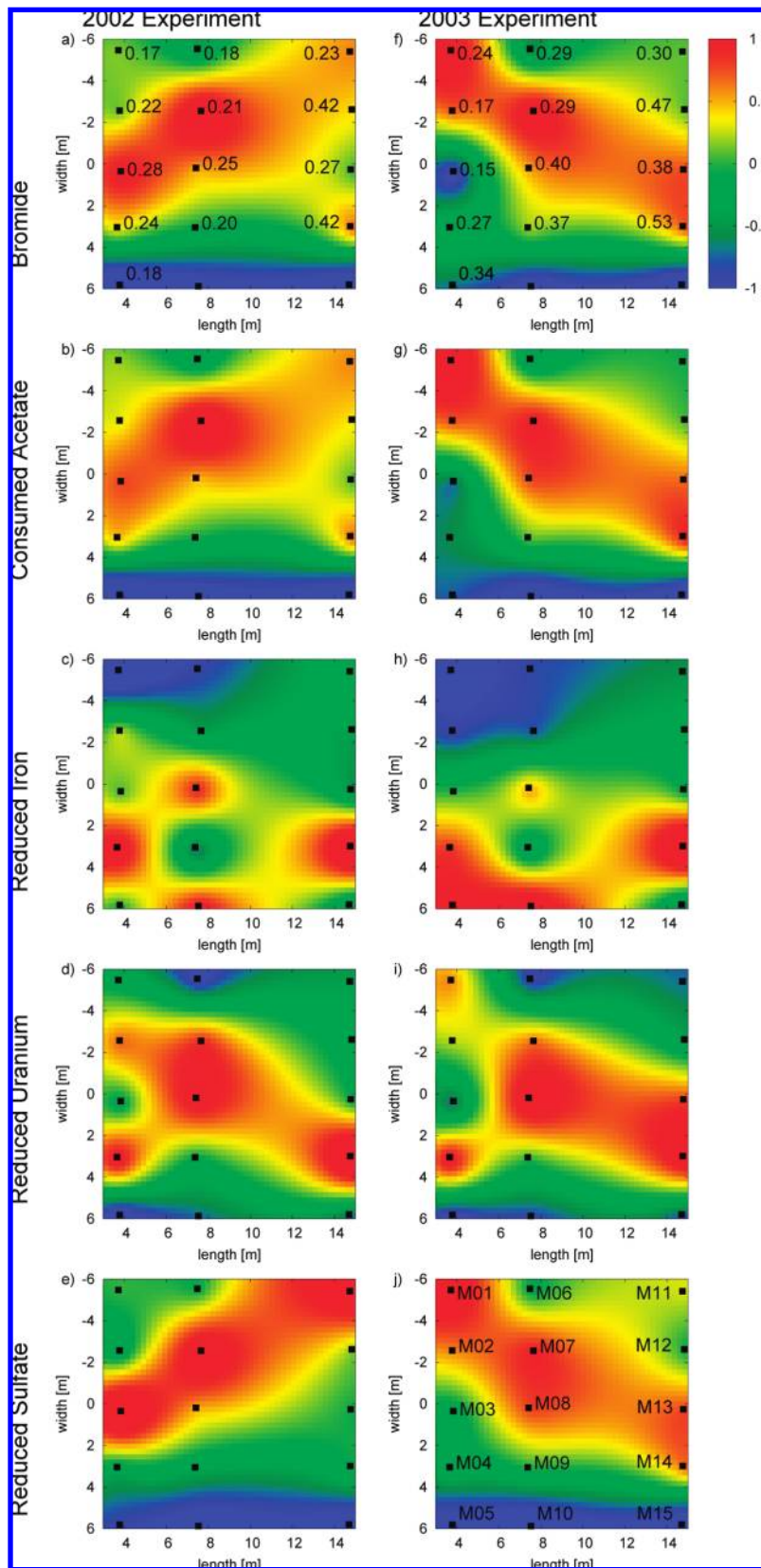


FIGURE 3. Contoured spatial patterns of the normalized apparent mass ( $m_a$ ) of bromide (a and f), consumed acetate (b and g), reduced iron (c and h), uranium (d and i), and sulfate (e and j) during the 2002 (left) and 2003 (right) biostimulation experiments. As result of the normalization, the color-bar is a measure of the standard deviation from the mean values and is dimensionless. The Figures encompass the area in Figure 1 that includes the 15 downgradient monitoring wells. Superimposed on the patterns of the normalized  $m_a$  of bromide (a and f), are the apparent velocities in m/d. The monitoring well names are superimposed in panel j.

in the 2003 experiment, the patterns of the  $m_a^{\text{norm}}$  of reduced uranium coincided ( $r = 0.80$ ) with those of the  $m_a^{\text{norm}}$  of

bromide (Figure 3f and i). This suggests that iron geochemistry may predominantly govern uranium reduction under low

acetate conditions whereas hydrological heterogeneity may dominate during the high acetate conditions.

## Discussion

We used a temporal moment analysis that relies on a streamtube approximation to characterize apparent velocity and masses of conservative and reactive species during two sequential biostimulation experiments. The apparent mass permitted integration over the time of an experiment and thus quantification of the accumulated responses (i.e., the iron, uranium, and sulfate reduction) of a subsurface system as a function of the introduced species (i.e., acetate and bromide). A benefit of the measure of the apparent mass is that no assumptions need to be made about the reaction kinetics during the estimation, while a limitation is that the temporal dynamics of the chemical reactions are lost due to the integration over time. The apparent mass provides spatial information about the status of the overall reactive transport in the direction of flow and about the relation between the hydrological and geochemical heterogeneity and the conservative and reactive transport processes in a direction perpendicular to the mean flow. The apparent masses of consecutive experiments provide temporal information about changes in the subsurface system.

Application of the developed approach to the two biostimulation experiments suggests that sulfate reduction was dominated by the hydrological heterogeneity and that the iron reduction was dominated by the geochemical heterogeneity of the subsurface. Uranium reduction showed variable behavior as a function of acetate injection. During relatively low acetate concentrations (2002 experiment), our results indicate that the uranium reduction was dominated by the geochemical heterogeneity, as the spatial distribution of the apparent mass was similar to the one of the iron reduction. During prolonged acetate injection (2003 experiment), our results indicated the uranium reduction was dominated by the hydrological heterogeneity, as was the sulfate reduction.

Significant changes in the apparent velocities and the apparent masses of bromide between the 2002 and 2003 experiments suggested that the hydrology of the system was modified as a result of the biostimulation experiment, perhaps due to clogging associated with the formation of biofilms, bioaggregates, and precipitates. Our interpretation is supported by ongoing reactive transport modeling of the Rifle IFRC biostimulation experiments that include the evolution of precipitates and biomass (14). This ongoing research suggests that the evolution of biomass, FeS, and calcite can lead to accumulations that may be sufficient to block pore throats and thus to alter flow characteristics.

Our study has shown that a temporal moment approach permits the quantification of the spatial and temporal distributions of the intensity of amendment delivery and of reactions and their relations to conservative transport characteristics. Through assessment of the spatial patterns of the flow and the apparent mass, new insights about the influence of hydrological and biogeochemical heterogeneity on the biostimulation experiments and their changes over time were developed. In particular, we illustrated that feedbacks between hydrological heterogeneity and bioremediation-induced biogeochemical transformations exist at the field scale. In addition to potentially impacting the efficacy and sustainability of contaminant remediation, such feedbacks could play an important role in other subsurface manipulations, such as enhanced oil recovery or carbon dioxide sequestration.

## Acknowledgments

Funding for this study was provided by the Environmental Remediation Science Program, Office of Biological and

Environmental Research, U.S. Department of Energy (DOE Grant DE-AC02-05CH11231) as part of the LBNL Sustainable Systems Science Focus Area. We sincerely thank Dr. Philip Long (PNNL) and the DOE Rifle, CO Integrated Field Research Center team for allowing us to work with their historical data set. We thank Dr. Steven Yabusaki (PNNL) for many fruitful discussions about hydrological gradients and data set nuances associated with the study site. We thank the three anonymous reviewers.

## Supporting Information Available

Additional figures and information. This material is available free of charge via the Internet at <http://pubs.acs.org>.

## Literature Cited

- (1) Lovley, D. R. Cleaning up with genomics: Applying molecular biology to bioremediation. *Nature Rev. Microbiol.* **2003**, *1*, 35–44, DOI: 10.1038/nrmicro731.
- (2) Scheibe, T. D.; Fang, Y.; Murray, C. J.; Roden, E. E.; Chen, J.; Chien, Y.-J.; Brooks, S. C.; Hubbard, S. S. Transport and biogeochemical reaction of metals in a physically and chemically heterogeneous aquifer. *Geosphere* **2006**, *2*, 220–235.
- (3) Hubbard, S.; Williams, K.; Conrad, M.; Faybishenko, B.; Peterson, J.; Chen, J.; Long, P.; Hazen, T. Geophysical monitoring of hydrological and biogeochemical transformations associated with Cr(VI) bioremediation. *Environ. Sci. Technol.* **2008**, *42*, 3757–3765. DOI: 10.1021/es071702s.
- (4) Baveye, P.; Vandevivere, P.; Hoyle, B.; DeLeo, P.; de Lozada, D. Environmental impact and mechanisms of the biological clogging of saturated soils and aquifer materials. *Crit. Rev. Environ. Sci. Technol.* **1998**, *28*, 123–191.
- (5) Thullner, M.; Mauclaire, L.; Schroth, M. H.; Kinzelbach, W.; Zeyer, J. Interaction between water flow and spatial distribution of microbial growth in a two-dimensional flow field in saturated porous media. *J. Contam. Hydrol.* **2002**, *58*, 169–189.
- (6) Seifert, D.; Engesgaard, P. Use of tracer tests to investigate changes in flow and transport properties due to bioclogging of porous media. *J. Contam. Hydrol.* **2007**, *93*, 58–71.
- (7) Kapellos, G. E.; Alexiou, T. S.; Payatakes, A. C. Hierarchical simulator of biofilm growth and dynamics in granular porous materials. *Adv. Water Resour.* **2007**, *30*, 1648–1667.
- (8) Seymour, J. D.; Gage, J. P.; Codd, S. L.; Gerlach, R. Magnetic resonance microscopy of biofouling induced scale dependent transport in porous media. *Adv. Water Resour.* **2007**, *30*, 1408–1420.
- (9) Wu, W. M.; Carley, J.; Fienen, M.; Mehlhorn, T.; Lowe, K.; Nyman, J.; Luo, J.; Gentile, M. E.; Rajan, R.; Wagner, D.; Hickey, R. F.; Gu, B. H.; Watson, D.; Cirpka, O. A.; Kitanidis, P. K.; Jardine, P. M.; Criddle, C. S. Pilot-scale in situ bioremediation of uranium in a highly contaminated aquifer. 1. Conditioning of a treatment zone. *Environ. Sci. Technol.* **2006**, *40*, 3978–3985.
- (10) Faybishenko, B.; Hazen, T. C.; Long, P. E.; Brodie, E. L.; Conrad, M. E.; Hubbard, S. S.; Christensen, J. N.; Joyner, D.; Borglin, S. E.; Chakraborty, R.; Williams, K. H.; Peterson, J. E.; Chen, J.; Brown, S. T.; Tokunaga, T. K.; Wan, J.; Firestone, M.; Newcomer, D. R.; Resch, C. T.; Cantrell, K. J.; Willett, A.; Koenigsberg, S. In situ long-term reductive bioimmobilization of Cr(VI) in groundwater using hydrogen release compound. *Environ. Sci. Technol.* **2008**, *42*, 8478–8485.
- (11) Anderson, R. T.; Vrionis, H. A.; Ortiz-Bernad, I.; Resch, C. T.; Long, P. E.; Dayvault, R.; Karp, K.; Marutzky, S.; Metzler, D. R.; Peacock, A.; White, D. C.; Lowe, M.; Lovley, D. R. Stimulating the in situ activity of *Geobacter* species to remove uranium from the groundwater of a uranium-contaminated aquifer. *Appl. Environ. Microbiol.* **2003**, *69*, 5884–5891.
- (12) Vrionis, H. A.; Anderson, R. T.; Ortiz-Bernad, I.; O'Neill, K. R.; Resch, C. T.; Peacock, A. D.; Dayvault, R.; White, D. C.; Long, P. E.; Lovley, D. R. Microbiological and geochemical heterogeneity in an in situ uranium bioremediation field site. *Appl. Environ. Microbiol.* **2005**, *71*, 6308–6318.
- (13) Yabusaki, S. B.; Fang, Y.; Long, P. E.; Resch, C. T.; Peacock, A. D.; Komlos, J.; Jaffe, P. R.; Morrison, S. J.; Dayvault, R. D.; White, D. C.; Anderson, R. T. Uranium removal from groundwater via in situ biostimulation: Field-scale modeling of transport and biological processes. *J. Contam. Hydrol.* **2007**, *93*, 216–235.
- (14) Li, L.; Steefel, C. I.; Kowalsky, M. B. Biogeochemical reaction kinetics associated with uranium bioremediation at multiple scales. *Eos Trans. AGU, Fall Meet. Suppl.* **2007**, H32D–03.

- (15) Kreft, A.; Zuber, A. Physical Meaning Of Dispersion-Equation And Its Solutions For Different Initial And Boundary-Conditions. *Chem. Eng. Sci.* **1978**, *33*, 1471–1480.
- (16) Harvey, C. F.; Gorelick, S. M. Temporal Moment-Generating Equations - Modeling Transport And Mass-Transfer In Heterogeneous Aquifers. *Water Resour. Res.* **1995**, *31*, 1895–1911.
- (17) Vanderborght, J.; Vereecken, H. Analyses Of Locally Measured Bromide Breakthrough Curves From A Natural Gradient Tracer Experiment At Krauthausen. *J. Contam. Hydrol.* **2001**, *48*, 23–43.
- (18) Jose, S. C.; Rahman, M. A.; Cirpka, O. A. Large-scale sand-box experiment on longitudinal effective dispersion in heterogeneous porous media. *Water Resour. Res.* **2004**, *40*, W12415.
- (19) Dagan, G.; Cvetkovic, V.; Shapiro, A. A solute flux approach to transport in heterogeneous formations 1. The general framework. *Water Resour. Res.* **1992**, *28*, 1369–1376.
- (20) Cvetkovic, V.; Shapiro, A. M.; Dagan, G. A solute flux approach to transport in heterogeneous formations. 2. Uncertainty analysis. *Water Resour. Res.* **1992**, *28*, 1377–1388.
- (21) Cirpka, O. A.; Kitanidis, P. K. Characterization of mixing and dilution in heterogeneous aquifers by means of local temporal moments. *Water Resour. Res.* **2000**, *36*, 1221–1236.
- (22) Vanderborght, J.; Kemna, A.; Hardelauf, H.; Vereecken, H. Potential of electrical resistivity tomography to infer aquifer transport characteristics from tracer studies: A synthetic case study. *Water Resour. Res.* **2005**, *41*, W06013, DOI: 10.1029/2004WR003774.
- (23) Bloem, E.; Vanderborght, J.; de Rooij, G. Leaching surfaces to characterize transport in a heterogeneous aquifer: Comparison between flux concentrations, resident concentrations, and flux concentrations estimated from temporal moment analysis *Water Resour. Res.* **2008**, *44*, W10412, DOI: 10.1029/2007WR006425.

ES803367N